

# Experimental Investigation on the Capacity of Steel Cold Formed RHS Tubular Stub Columns with A Central Circular Web Opening

Hanan H. Eltobgy<sup>1</sup>, Fathy A. Abdelfattah<sup>1</sup>, Emad Darwish<sup>1</sup>, Hisham Farag<sup>1,\*</sup>

<sup>1</sup> Faculty of Engineering at Shoubra, Benha University, Cairo, Egypt.

\*Corresponding author

E-mail address: [hanan.altobgy@feng.bu.edu.eg](mailto:hanan.altobgy@feng.bu.edu.eg), [fathy.aboelala@feng.bu.edu.eg](mailto:fathy.aboelala@feng.bu.edu.eg), [emad.darwish@feng.bu.edu.eg](mailto:emad.darwish@feng.bu.edu.eg), [hisham.hassan@feng.bu.edu.eg](mailto:hisham.hassan@feng.bu.edu.eg)

**Abstract:** The capacity of rectangular hollow section (RHS) cold-formed stub columns with two opposing central circular openings at column mid-height was experimentally studied in this research. The selected stub columns had a minimum yield strength of 357 MPa. The impact of two opposing central circular openings on the structural performance of tubular steel stub columns was examined for perforation size to flat-width ratios of 0.4 and 0.6. Also, these columns with openings were strengthened with a doubler plate. This study presents the ultimate column abilities, load-end shortening curves, regional geometric faults, and typical failure modes extracted from the current test program. Further, this paper has presented a study of the potential of strengthening the RHS stub columns by using external doubler plates with two distinct heights with doubling and tripling the aperture diameter. As for the cold-formed thin-walled steel stub column strengthened with external doubler plates, the larger the doubler plate height, the greater the improvement of the load ability. The ultimate buckling load capacity of the strengthened perforated rectangular hollow section (RHS) under axial compression is increased by up to 40%.

**Keywords:** Cold-formed, Rectangular Hollow section (RHS), Experimental Study, structural behavior; Capacity; Strengthening.

## 1. Introduction

Besides aesthetic properties, tubular profiles have numerous advantages over open profiles, such as high compressive strength, bending, and torsional strength, which encourage their usage in many industrial, commercial, and residential buildings [1, 2]. Structural members (beams and columns) are perforated (or cutouts, holes, openings) to accommodate different modifications and needs, such as Concealed electrical and signal lines, heating and cooling air circulation, inspection, and maintenance work (especially for bridges and towers), freshwater and wastewater installations, connections to other members, etc. aesthetic appearance, and material optimization. However, the load transmission process may be affected by the addition of perforations in a tubular structural part. Because of the various cases of fabrication, there could be a redistribution of strains that would lead to stress concentration and localized collapse at the perforation. [7,10]. Numerous studies on steel plates [6,11–12], beams [4,13–14], and columns [3, 5, 8, 9, 10,15–20]) studying the impact of holes on member strength capacity have been published since the late 1950s. Further, in their study of the symmetric progressive buckling load of thin-walled mild steel square tubes with circular perforations, [18] found that the buckling load decreased linearly with increasing perforation diameter. Further, [19] investigated the effects of the size and placement of rectangular perforations on the ultimate strength of lipped channel steel stub columns. They found that the strength of a thin channel column could be significantly reduced if the perforation is

in the effective area, but that the strength was found to be hardly affected by perforations in the ineffective area. [6] concluded that steel plates with circular perforations have higher capacities than those with square perforations based on the findings of the finite element (FE) analysis of steel plates with either circular or square perforations. Further, they set a design equation to determine the load capacity for perforated equal-angle stub columns using the FE results. Through a thorough parametric investigation using FE analysis, [5] created a simple design equation to predict the maximum capacity of plain and lipped channel sections with circular holes. Further, using both experimental and numerical methods, [15] investigated the impact of elliptical perforations on performing thin cylindrical shells subjected to axial load and provided an empirical formula to calculate the buckling capacity. Further, the reduction in post-peak ductility was investigated by [16], who also noted that including slotted holes in lipped channel stub columns had a minimal impact on ultimate strength. [3] extended the design expressions for cold-formed steel columns with perforations into six alternative possibilities by modifying the Direct Strength Method (DSM) specified in North American Specification (NAS 2007) [21] using seventy-eight tests and 213 FE column strength data. The North American Specification (NAS 2012) [22] was found to use Design Option 4 (where the local buckling capacity was restricted to net area-based yield capacity) [22]. By considering parameters like perforation shapes, sizes, and spacings using the isoperimetric spline finite strip method (ISFSM), [9] investigated the inelastic stress distributions, load transfers, and failure modes on perforated plates and

C-section columns in compression and concluded that perforation shape has a negligible impact on the ultimate capacity of columns. Based on FE research, [17] found that a single circular perforation at the mid-height of a circular stub column resulted in the greatest reduction in column buckling load. To evaluate the impact of perforation characteristics, such as perforation sizes and spacings, on the load capacities of open cross-sections, Yao, and Rasmussen [10] conducted a thorough parametric analysis. Based on the column strength data from [10], the accuracy of the design equations of DSM described in AS/NZS 4600 [23], Design Option 4 proposed by Moen and Schafer [3], and 2 out of 19 design alternatives proposed by Yao and Rasmussen [24] was assessed. To determine the stub column capacity of square hollow sections (SHS) and rectangular hollow sections (RHS) with opposing imperative round perforations at column mid-top, [25,26,27] conducted an experimental investigation. They discovered that the final capacity of SHS/RHS stub columns was unaffected by a central porosity ratio ( $d/w$ ) up to 10%. The breaking load of perforated SHS/RHS stub columns is, therefore, not affected by using a smaller perforation size ( $d 0.1w$ ). They concluded that most of the design equations available now conservative ones. The effect of perforations on thin cylinders were researched by [28]. They presented test and verification findings for the FEM simulation. Both a hollow circular section with 12 circular holes and a semi round tube with no holes were considered. They subjected the specimen and the FEM model to compression, bending, and torsional loads. The strain gauge records agree with the FEM findings for the perforated model. They discovered that the FEM findings and the strain gauge records are in good agreement with the perforated model under torsional loading. An experimental investigation was presented by [29] to examine the effects of an opening section on the stability and strength of steel columns with cold-formed thin sections (CFS) under axial compression load. They concluded that for struts with box and channel sections, respectively, the greatest drop in axial compressive strength of struts induced by the existence of web apertures is found to be about 30% and 45% of the reference strut strength. They concluded that web apertures reduced the axial compressive strength of the column specimens less for circular openings than for rectangular and/or square web openings. Further, using both experimental and numerical methods, [30] investigated the behavior and design of thin, non-compact steel square hollow sections (SHS) under eccentric loading. He discovered that the usual equation for slender sections is 40% more cautious than test and numerical results in several circumstances, particularly when the slenderness ratio is less than 1.0. He also concluded that they should change the design formulae currently used for elongated SHSs under eccentric stress. He therefore put down a modern design equation for these kinds of portions. Further, to forecast the load-bearing and rotational capacities of steel members subjected to bending and axial stresses, [31] conducted two types of experimental testing and collaborative analysis operations. They concluded that the

column's base experienced localized buckling, which indicated the failure process. The moment load capacity and the rotational capacity is both decreased by increasing the dimensionless axial load. They also concluded that the moment-bearing and rotational capacities are significantly influenced by the material parameters. Further, a relatively new sort of thermal profile with stretched perforations that resemble a net was studied by [32]. They discussed how perforated CFS-C profiles buckled under compressive pressure. They concluded that it also seemed reasonable to employ computer modelling to consider the original geometrical faults of the sections given how susceptible such perforated CFS structures are to mechanical deformation.

The main purpose of the current study is to investigate the effect of strengthening the perforated RHS stub columns by using external doubler plates with two distinct heights with doubling and tripling the aperture diameter under axial static compressive load, one of the commercially available RHS sections was chosen carefully with the standard section dimensions as shown in Fig. 1 to be used in the experimental work, Also the increase in the axial compressive strength of the column specimens caused by doubler plates for different strengthening ratios has been studied.

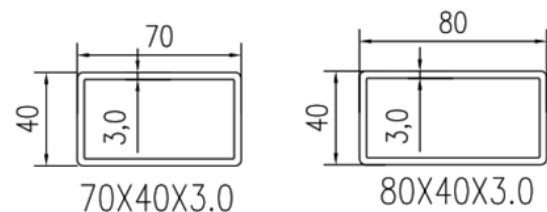


Figure 1. tube Cross-section used in experimental work..

## 2. EXPERIMENTAL STUDY

### 2.1 Experimental program

An experimental program was carried out to investigate the effects of web opening on the behavior and failure of steel stub columns with cold-formed thin-walled sections (CFS) subjected to axial static compressive load. The dimension labelling system used in this paper is shown in Fig. 2.a, where B, D, t, d, w, r, and L represent the width, depth, thickness, diameter of perforation, flat-width, outer corner radius, and stub column height.

Fourteen tested steel columns specimens have a tubular section with two different dimensions; Seven specimens have a tubular section with dimensions of RHS (70×40×3) mm (width × depth × thickness). The other seven specimens with dimensions of RHS (80×40×3) mm. The effect of the size of two opposing central circular web opening diameters was investigated. Specimen were strengthened with doubler plates fig 2. b, every seven columns with the same cross-section shape was divided into three groups of two columns beside the reference column that has no web openings:

**Group I:** include stub column specimens without strengthening, including the reference column that has no web openings. (6 Specimens)

**Group II:** strengthened specimens by adding a doubler plate with height  $S=2d$ . (4 Specimens)

**Group III:** strengthened specimens by adding a doubler plate with height  $S=3d$ . (4 Specimens)

All groups of columns have two (d/w) ratios; 40% and 60% opening area that are located at the mid-height of the column web.

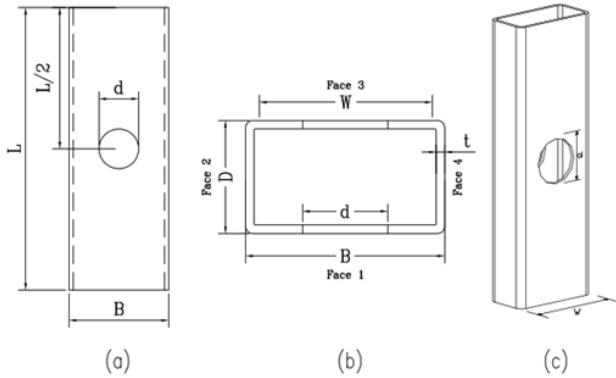


Figure 2.a column stub dim used in experimental work.

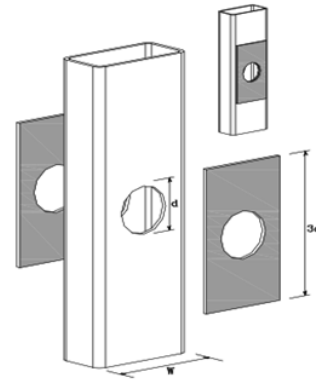


Figure 2.b column stub strengthening 2d, 3d used in experimental work.

Table 1 stands for the Specimens grouping with the labeling code (ID).

The test program is conducted to study the effect of the hole diameter (d), (d/w), and the doubler plate height, stiffening ratio on the column axial capacity.

The label of the test specimens is designed such that the element dim, ratio (d/w), and (s) ratio are defined. An example of a specimen label (ID) is given below.

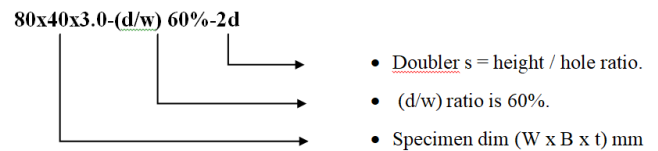


Table 1. Test Matrix of Specimens Tested in Group I, II and III.

Group	S.N	mark	Specimen ID	W x B x t mm	d/w%	d = hole dia. mm	s = doubler height mm
I	1	20	70x40x3.0-(d/w) 00%-0d	70x40x3.0	0	0	0
	2	23	70x40x3.0-(d/w) 40%-0d	70x40x3.0	40	28	0
	3	25	70x40x3.0-(d/w) 60%-0d	70x40x3.0	60	42	0
	4	39	80x40x3.0-(d/w) 00%-0d	80x40x3.0	0	0	0
	5	42	80x40x3.0-(d/w) 40%-0d	80x40x3.0	40	32	0
	6	44	80x40x3.0-(d/w) 60%-0d	80x40x3.0	60	48	0
II	7	29	70x40x3.0-(d/w) 40%-2d	70x40x3.0	40	28	56
	8	31	70x40x3.0-(d/w) 60%-2d	70x40x3.0	60	42	84
	9	48	80x40x3.0-(d/w) 40%-2d	80x40x3.0	40	32	64
	10	50	80x40x3.0-(d/w) 60%-2d	80x40x3.0	60	48	96
III	11	35	70x40x3.0-(d/w) 40%-3d	70x40x3.0	40	28	84
	12	37	70x40x3.0-(d/w) 60%-3d	70x40x3.0	60	42	126
	13	54	80x40x3.0-(d/w) 40%-3d	80x40x3.0	40	32	96
	14	56	80x40x3.0-(d/w) 60%-3d	80x40x3.0	60	48	144

**2.2 Material properties (Coupon test)**

The stub columns were made from commercially available sections of tubular columns in Egypt. Steel materials used to form the tubular elements have undergone tensile coupon testing to define its mechanical properties. The standard tensile test of the coupon specimen was conducted according to ASTM E 8M/16. Specimens were cut from the webs of the parent elements of the used tubes. A typical stress-strain curve for the two coupon tests is shown in Figs. 3.

The Material properties are summarized in Table 2. The value of the yielding stress  $\sigma_0 = 357$  MPa and ultimate stress  $\sigma_u = 399$  MPa are considered in the research.

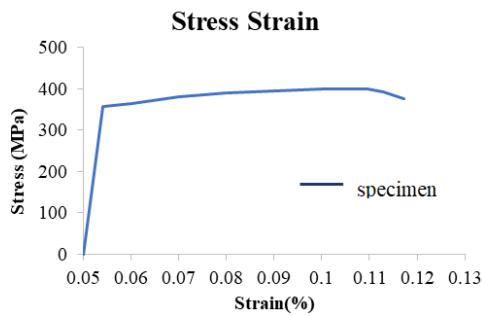


Figure 3. Stress-strain curve

**2.3 Specimens' preparation**

Fourteen steel columns with cold-formed RHS of dimension 80x40x3 and 70x40x3 of a total length of  $L = 200$  mm have been considered in the experimental tests.

The opposite holes at the samples mid height were cut with a laser CNC machine to produce perfect circular holes fig 4. The Doublor plate was cut from the same primary tubular column, giving it the same material characteristics and thickness as the base metal, figs 5 and 6. The samples were combined with the Doublor plate using full-length GMAW welding. The bearing plates were then welded to the samples to disperse the loads from the pressing machine fig 7.



Figure 4. Detaching components



Figure 5. Fitting of the two element parts.



Figure 6. Assembling element parts.



Figure 7. welding parts (Final specimen).

**2.4 Test Setup**

All the specimens were evaluated with simply supported boundary conditions at both ends. The load is provided by a hydraulic jack and aligned vertically on the element. The load cell used for the experiments is calibrated before the testing procedure. Thick steel bearing plates were used at the upper and lower sides of the specimen to insure uniform load distribution. A typical experimental setup is shown in Figs. 8,9, and 10.

Table 2. Test Matrix of Specimens Tested in Groups I, II, and III

Coupon	Tube	w (mm)	t (mm)	$L_c$ (mm)	E (GPa)	$\sigma_0$ (MPa)	$\sigma_u$ (MPa)
743	70 x 40 x 3.0	30	3.0	300	199	357	399
744	80 x 40 x 3.0	30	3.0	300	199	358	399



The ultimate capacity of solid, perforated, and strengthened stub columns was calculated using a 400 kN hydraulic loading frame. The specimens were subjected to a concentric incremental load using the load control procedure in the testing machine at a constant loading rate of 1.0 kN/s. Two linear variable displacement transducers (LVDTs) with stroke lengths of 80 mm were used to measure the end-shortening of the stub columns. An initial load of 1.0 kN was applied to ensure full contact between the specimen edges and the bearing plates. The concentric incremental load was applied up to a certain point until enough post-ultimate range was captured. The readings from load cells, and displacement transducers were recorded at regular intervals.



Figure 8. Specimen ends connection.

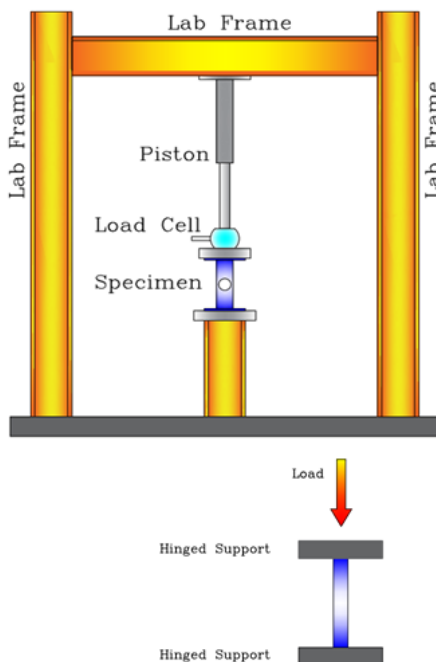


Figure 9. Test setup.

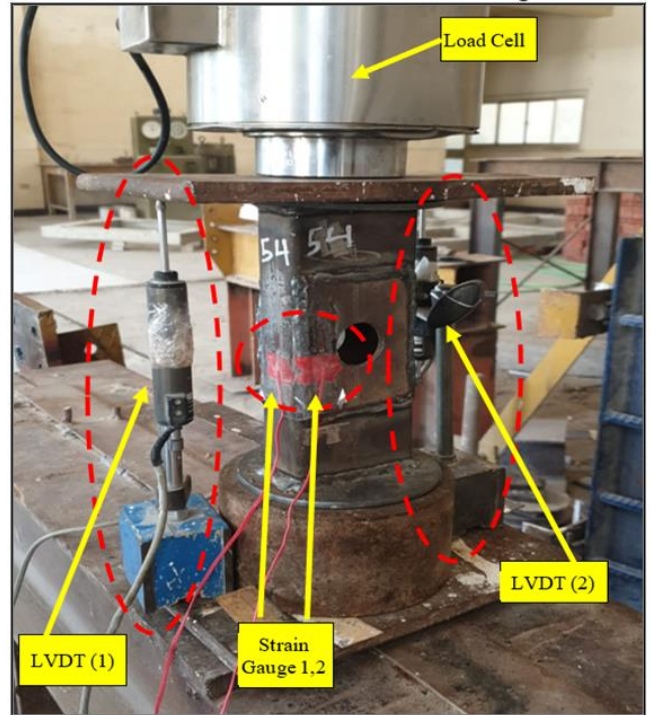


Figure 10. Arrangement of LVDTs and Strain Gauges on the tested specimen.

### 3. TEST RESULTS, VERIFICATION, AND DISCUSSION

The failure modes, ultimate axial compressive load, and load-displacement behavior are presented and discussed in the following sections. The load capacity of the tested steel closed and perforated stub is compared and verified against the AISI standard, as well as the perforation ratio at Tekcham Singh and Konjengbam Singh [25] experimental results.

#### 3.1 Ultimate Load Capacity verification

In this section, the load capacity of the tested steel closed and opened stubs of (Group I) are presented, and a comparison with verification against the AISI standard [34] and experimental results will be conducted.

The recorded test results of the group I specimens are summarized in Table 3. The Experimental ultimate load for the closed and perforated stub column specimens ( $P_{Exp,C}$ ,  $P_{Exp,O}$ ), and the end shortening ( $\Delta$ ) are shown in column 3. Also, Table 3 presents the nominal axial load ( $P_n$ ) for the closed stub column determined according to the AISI standards [34] and the reduction factor R of perforation ratio determined by Tekcham Singh and Konjengbam Singh [25] are recorded, where R is the load capacity of opened sample relative to the closed one. It can be concluded that there is a good agreement between the experimental results and the AISI design code [34], as well as experimental results.

**Table 3.** Test Matrix of Specimens Tested in Group I.

Group	Specimen	Experimental		AISI Code		Reduction Factor Comparison [25]			
		$P_{Exp.C}$	$P_{Exp.O}$	$\Delta$	$P_n$	$\frac{P_n}{P_{Exp.C}}$	$R_{exp}$	$R_{Singh}$	%
		(kN)	(kN)	(mm)	(kN)	$\frac{P_{Exp.O}}{P_{Exp.C}}$	$\frac{P}{P_O}$	$\frac{R_{exp}}{R_{Singh}}$	
I	70x40x3.0- (d/w) 00%-0d	247.15		1.87	208.41	0.84	-		
	70x40x3.0- (d/w) 40%-0d		223.38	3.17			0.90	0.89	102%
	70x40x3.0- (d/w) 60%-0d		168.89	3.85			0.68	0.69	99%
	80x40x3.0- (d/w) 00%-0d	260.84		3.48	229.67	0.88	-	-	
	80x40x3.0- (d/w) 40%-0d		223.83	3.5			0.86	0.89	99%
	80x40x3.0- (d/w) 60%-0d		186.01	2.63			0.71	0.69	100%
Overall Mean						0.86	0.79	0.79	
40% Mean							0.88	0.89	
60% Mean							0.70	0.69	

### 3.1.1 Design force Code AISI Standard

The American Iron and Steel Institute (AISI S100-16) [34] provides design formulae to estimate the column capacity of cold-formed steel structural members using the Effective Width Method (EWM) and Direct Strength Method (DSM). The nominal axial strength of a member in compression shall be the minimum of the axial capacity of a member for yielding and global buckling ( $P_{ne}$ ), local buckling interacting with yielding and global buckling ( $P_{nl}$ ), and distortional buckling ( $P_{nd}$ ), according to Section E of AISI S100-16 [34]. Because doubly symmetric closed sections chosen are relatively thick in the current experimental program, distortional buckling capacity is large and thus ignored.

#### 3.1.1.1 Global buckling determination

The nominal axial capacity ( $P_{ne}$ ) for yielding and global buckling is estimated based on Section E2 of AISI S100-16 [34] as follows:

$$P_{ne} = A_g F_n \quad (1)$$

In which,

$A_g$  = gross cross-sectional area,

$F_n$  = compressive stress and calculated as follows:

$$\begin{aligned} \text{For } \lambda_c \leq 1.5; \quad F_n &= (0.658\lambda_c^2) f_y \\ \text{For } \lambda_c > 1.5; \quad F_n &= \left(\frac{0.877}{\lambda_c^2}\right) f_y \end{aligned} \quad (2)$$

where,

$$\lambda_c = \sqrt{f_y / F_{cre}}, \quad F_{cre} = \frac{\pi^2 E}{(KL/r)^2}$$

$F_{cre}$  = Elastic global buckling stress estimated based on Appendix 2 of AISI S100-16 [34],  $f_y$  = Yield Stress.

#### 3.1.1.2 Local buckling determination

The nominal axial capacity ( $P_{nl}$ ) for local buckling interacting with yielding and global buckling is calculated based on either EWM in Section E3.1 or DSM on Section E3.2 of AISI S100-16 [34].

Local buckling determination is based on Effective Width Method, ( $P_{nl,EWM}$ ). The nominal axial capacity for local buckling ( $P_{nl,EWM}$ ) based on Effective Width Method (EWM) is estimated using Eq. (3) given as follows:

$$P_{nl,EWM} = A_e F_n \leq P_{ne} \quad (3)$$

In which,

$P_{ne}$  and  $F_n$  are defined in Eqs. (1) and (2) respectively,

$A_e$  = Effective area is calculated by multiplying the member thickness by the sum of the effective width,  $b$ , of each element comprising the cross-section plus corner portions, assuming that corner portions are fully effective.

As shown in Table 3, The nominal axial strength ( $P_n$ ) for closed RHS given by AISI Standard is lower than the test ( $P_{Exp.C}$ ) as the maximum difference is 15%.

This result was also reported by [35], probably as a result of a conservative prediction of the stub column strength.

### 3.1.2 Effect of perforation

Table 3 presents the reduction in the column capacity  $R_{Exp}$  due to the introduction of perforation in the tested specimens.  $R_{Exp}$  was assessed by normalizing the perforated (opened) column capacities, ( $P_{Exp.O}$ ) from the test, with the corresponding closed stub column capacities, ( $P_{Exp.C}$ ) of similar cross-sectional dimensions. Also, the

reduction factor  $R_{Singh}$  [25]  $\frac{P}{P_0}$  for the same opening ratio  $d/w$  determined by [25] is recorded.

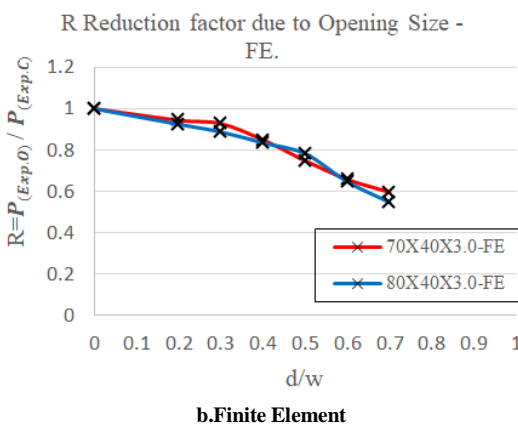
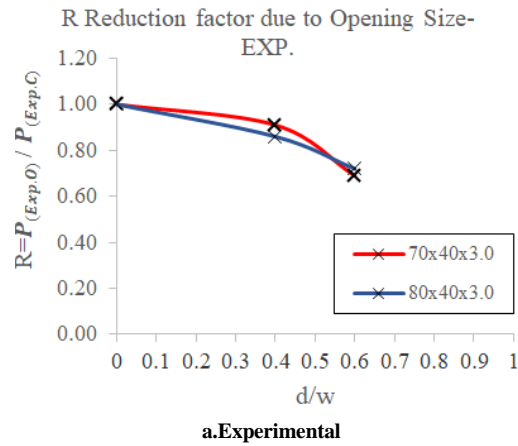


Figure 11. Impact of perforation size on column strength Group I

The plot of the normalized perforated stub column experimental capacities against the perforation size ratio,  $(d/w)$  for the specimen Group I is shown in figure 11.a. It can be noticed that the reduction in the ultimate capacities varies from 90% to 69% for perforation size ratio ranging from 40% to 60%. An overall, non-linear drop in the member capacity was observed as the perforation size increases. This is due to the lack of stiffness and the effective cross-sectional area. Furthermore, the authors have carried

out a finite element parametric study, and the results will be published in a future article. Some of the results for six samples are presented in fig.11.b for sake of comparison. From fig.11.b it can be concluded that; the reduction in ultimate capacities ranges from 85% to 64% for perforation size ratios ranging from 40% to 60%, with a 5% variance from the results of the experiment.

These conclusions are consistent with those reached by Tekcham Singh and Konjengbam Singh [25].

### 3.2 Failure Modes

Figs. 12, 13, 14, and 15 show the tested steel column specimens at failure. Local buckling occurred at various locations along the length of all tested columns, depending on opening diameter and web opening strengthening. The five failure modes of the tested steel column specimens are summarized in Tables 4 and 5.

The local buckling of the closed steel columns was located at the ends of the column, as shown in Figs 12.a to 15.a, whereas the local buckling for the specimens with opening  $d/t = 40\%$  was located in the middle of the column length around the hole, as shown in Figs 12.b to 15.b. When the openings increased from  $d/t = 40\%$  to  $60\%$ , the columns buckling failure mode was lateral distortion buckling due to the reduction in the column axial stiffness, also the specimens are more sensitive to local geometry imperfections. The column axial stiffness is considerably reduced, and the column exhibits less axial strength.

Figs. 12.c, 12.d, 14.c, and 14.d show that the local buckling occurred at the columns end for the tested strengthened specimens with 2d or 3d for columns with opening ratio of 40%, because the doubler plates prevent the local buckling around the holes like the closed section.

On the other hand, Figs. 13.c, 13.d, 15.c, and 15.d show that for the tested strengthened specimens with 2d or 3d for an opening ratio of 60%, the doubler plate can't prevent even the local buckling or lateral distortion but also there is extra local buckling at the end of the column, combining mode 01 with mode 02 and mode 01 with 03 for 2d and 3d respectively.

The specimen's failure modes matrix is presented in table 4.



a) 70x40x3.0-(d/w)00%-0d b) 70x40x3.0-(d/w)40%-0d c) 70x40x3.0-(d/w)40%-2d d) 70x40x3.0-(d/w)40%-3d  
Figure 12. 70x40x3.0 – w/t 40%





a)70x40x3.0-(d/w)00%-0d b)70x40x3.0-(d/w)60%-0d c)70x40x3.0-(d/w)60%-2d d)70x40x3.0-(d/w)60%-3d

**Figure 13.** 70x40x3.0 – w/t 60%



a)80x40x3.0-(d/w)00%-0d b)80x40x3.0-(d/w)40%-0d c)80x40x3.0-(d/w)40%-2d d)80x40x3.0-(d/w)40%-3d

**Figure 14.** 80x40x3.0 – w/t 40%



a)80x40x3.0-(d/w)00%-0d b)80x40x3.0-(d/w)60%-0d c)80x40x3.0-(d/w)60%-2d d)80x40x3.0-(d/w)60%-3d

**Figure 15.** 80x40x3.0 – w/t 60%

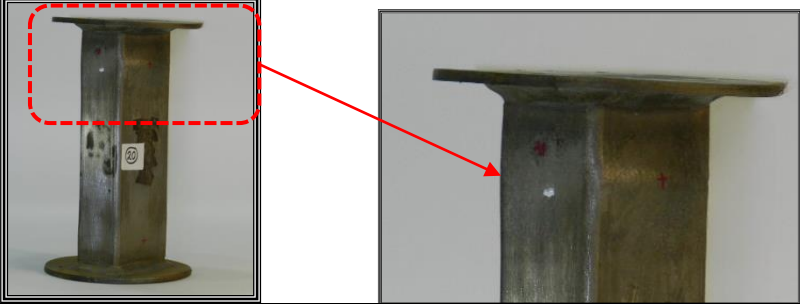
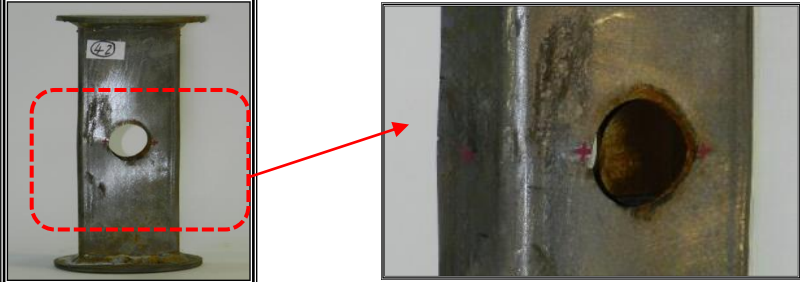
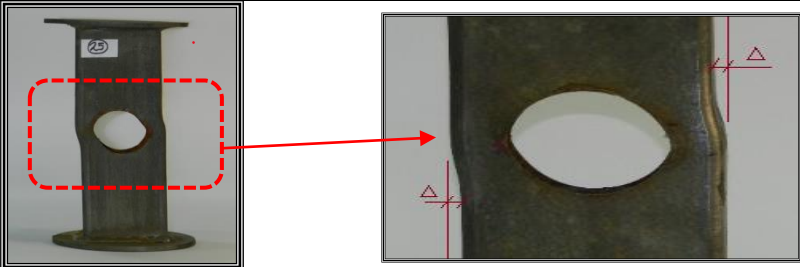


**Table 4.** Failure modes Matrix of Specimens Tested in Group I, II and III

Group	Mark	Specimen ID	MODE 01	MODE 02	MODE 03	MODE 04	MODE 05
I	20	70x40x3.0-(d/w) 00%-0d	•				
	23	70x40x3.0-(d/w) 40%-0d		•			
	25	70x40x3.0-(d/w) 60%-0d			•		
	39	80x40x3.0-(d/w) 00%-0d	•				
	42	80x40x3.0-(d/w) 40%-0d		•			
	44	80x40x3.0-(d/w) 60%-0d			•		



II	29	70x40x3.0-(d/w) 40%-2d	•	
	31	70x40x3.0-(d/w) 60%-2d		•
	48	80x40x3.0-(d/w) 40%-2d	•	
	50	80x40x3.0- (d/w) 60%-2d		•
III	35	70x40x3.0- (d/w) 40%-3d	•	
	37	70x40x3.0- (d/w) 60%-3d		•
	54	80x40x3.0- (d/w) 40%-3d	•	
	56	80x40x3.0- (d/w) 60%-3d		•

Table 5. Failure Mode Types.

MODE 01	Local Buckling at Ends	
MODE 02	Local buckling around the hole at mid height.	
MODE 03	Lateral distortion	
MODE 04	Combined local buckling at ends and local buckling around the hole at mid height. (Mode 01 + Mode 02)	
MODE 05	Combined of Local Buckling at Ends and Lateral Distortion (Mode 01 + Mode 03)	

### 3.3 Ultimate Load Capacity for columns with Strengthened Doubler plates

Tables 6 and 7 show the ultimate axial compressive load at failure for each steel column specimen listed in Table 2. These tables clearly show that the strengthening with Doubler plates significantly affected the column axial compressive strength for both 40% and 60% web opening ratio (d/w) steel column sections.

The results show that for both column sections tested, a ratio of opening width to total section width (d/w) of 40% results in a greater mean increase of axial compressive strength caused by the presence of Doubler plates than a ratio of 60% (d/w), with mean values of 108% and 101%, respectively, compared to the reference steel design load for the closed column.

The maximum percentage of the increase in the axial compressive strength in columns with (d/w) 40% due to the

presence of 2d Doubler plates are about 105% and 98% for both RHS70x40x3.0 and RHS80x40x3.0, respectively, while it noticed to be 110% and 102% for the same opening ratio but with 3d Doubler plates.

Moreover, Table 6 and 7 also show that, the increase in the axial compressive strength in columns with (d/w) 60% due to the presence of 2d Doubler plates are about 99% and 94% for both RHS70x40x3.0 and RHS80x40x3.0, respectively, while it is noticed to be 102% and 100% for the same opening ratio but with 3d Doubler plates

On the other hand, for both column sections considered in the experimental test, to reach about 98% or 100% of the designed axial compressive strength computed with AISI standard, for 40% (d/w) opening ratio using 2d Doubler plate is more effective and economic rather than 3d Doubler plate, which is more sufficient for larger opening 60% (d/w).

**Table 6.** Test results of Specimens 70x40x3.0 Tested in Group I, II and III

GROUP	Specimen	Experimental				Code AISI	Ratios Comparison								
		$P_{exp.c}$ (kN)	$P_{exp.o}$ (kN)	$P_{exp.s}$ (kN)	$\Delta$ (mm)		$P_n$ (kN)	d/w = 40%			d/w = 60%				
						$\frac{P_{Exp.S}}{P_{Exp.O}}$		$\frac{P_{Exp.S}}{P_{Exp.C}}$	$\frac{P_{Exp.S}}{P_n}$	$\frac{P_{Exp.S}}{P_{Exp.O}}$	$\frac{P_{Exp.S}}{P_{Exp.C}}$	$\frac{P_{Exp.S}}{P_n}$			
I	70x40x3.0-(d/w) 00%-0d	247.2			1.87	208.41									
	70x40x3.0-(d/w) 40%-0d		223.38		3.17										
	70x40x3.0-(d/w) 60%-0d		168.89		3.85										
II	70x40x3.0-(d/w) 40%-2d			243.97	2.08		1.09	0.99	1.17						
	70x40x3.0-(d/w) 60%-2d			231.5	2.34					1.37	0.94	1.11			
III	70x40x3.0-(d/w) 40%-3d			257.3	1.56		1.15	1.04	1.23						
	70x40x3.0-(d/w) 60%-3d			237.41	7.09					1.41	0.96	1.13			
Mean							1.12	1.01	1.20	1.39	0.95	1.12			

**Table 7.** Test results of Specimens 80x40x3.0 Tested in Group I, II and III

GROUP	Specimen	Experimental				Code AISI	Ratios Comparison								
		$P_{exp.c}$ (kN)	$P_{exp.o}$ (kN)	$P_{exp.s}$ (kN)	$\Delta$ (mm)		$P_n$ (kN)	d/w = 40%			d/w = 60%				
						$\frac{P_{Exp.S}}{P_{Exp.O}}$		$\frac{P_{Exp.S}}{P_{Exp.C}}$	$\frac{P_{Exp.S}}{P_n}$	$\frac{P_{Exp.S}}{P_{Exp.O}}$	$\frac{P_{Exp.S}}{P_{Exp.C}}$	$\frac{P_{Exp.S}}{P_n}$			
I	80x40x3.0-(d/w) 00%-0d	260.8			3.48	229.67									
	80x40x3.0-(d/w) 40%-0d		223.83		3.5										
	80x40x3.0-(d/w) 60%-0d		186.01		2.63										
II	80x40x3.0-(d/w) 40%-2d			251.7	3.43		1.12	0.96	1.09						
	80x40x3.0-(d/w) 60%-2d			242.84	3.78					1.31	0.93	1.06			
III	80x40x3.0-(d/w) 40%-3d			263.07	1.63		1.18	1.01	1.14						
	80x40x3.0-(d/w) 60%-3d			256.93	4.77					1.38	0.99	1.11			
Mean							1.15	0.99	1.11	1.34	0.96	1.09			

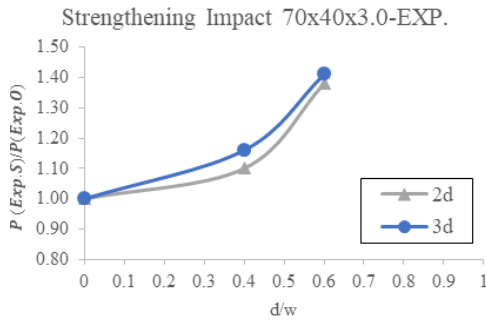


Figure 16. Impact of opening size on column strength RHS 70x40x3.0

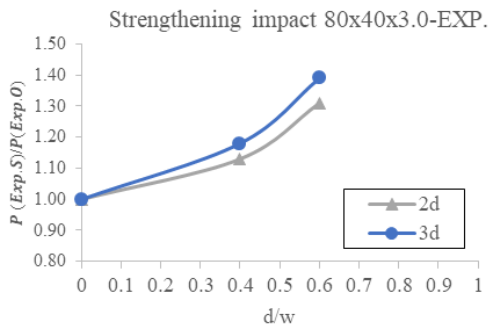


Figure 17. Impact of opening size on column strength RHS 80x40x3.0

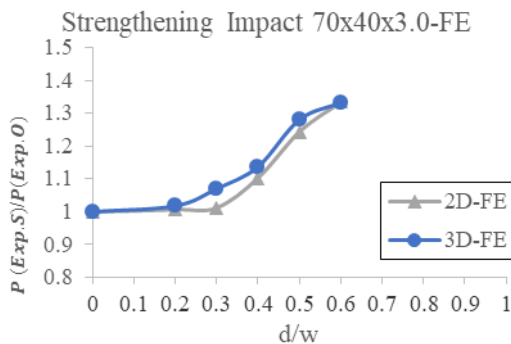


Figure 18. Impact of opening size on column strength RHS 70x40x3.0 Finite Element

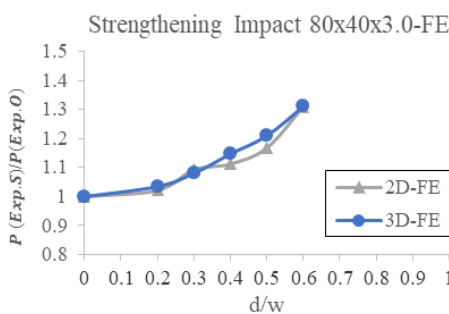


Figure 19. Impact of opening size on column strength RHS 80x40x3.0 Finite Element

### 3.4 Columns Ultimate Load Capacity and End Shortening

Table 6 and Table 7 show that the maximum percentage of the mean increases in axial strength due to the presence of doubler plates was almost identical for both RHS 70X40X3.0 and RHS 80X40X3.0 sections, which are%12 and%15 for Doubler plate with 2d, respectively, and 39% and 34% for Doubler plate with 3d.

Figs. 16 and 17 present the impact of strengthening compared to the opening size on the axial column experimental strength. The ultimate axial column strength increased by about 40% when using strengthening with doubler plates. Furthermore, the authors have carried out a finite element parametric study, and the results will be published in a future article. Some of the results for six samples are presented in fig.18 and fig.19 for sake of comparison. From fig.18 and fig.19 it can be concluded that; increases in axial strength due to the presence of doubler plates was almost identical for both RHS 70X40X3.0 and RHS 80X40X3.0 sections, which are%10 to %31 for Doubler plate with 2d, respectively, and 14% and 33% for Doubler plate with 3d, with a 5% variance from the results of the experiment.

This section presents the effect of strengthening using Doubler plates on the axial

compressive strength to axial displacement relationship of the tested steel columns for different sizes of web openings and for different strengthening ratios RHS.

Fig. 18 to Fig. 21 show the effect of the strengthening on the axial compressive strength and the axial displacement of the tested steel columns for the different lengths of doubler plates S=2d and S=3d for RHS 70x40x3.0 and 80x40x3.0 sections.

Fig. 18 and Fig. 19 show that for both RHS 70x40x3.0 and RHS 80x40x3.0 sections column with web opening ratio of 40%, steel columns strengthening with doubler S=2d improves the axial compressive strength without increasing columns stiffness, whereas columns strengthening with doubler S=3d improves both axial compressive strength and axial stiffness.

Fig. 20 show that for RHS 70x40x3.0 section column with web opening ratio of 60%, steel columns strengthening with doubler S=2d improves both axial compressive strength and axial stiffness, whereas columns strengthening with doubler S=3d improves only the axial compressive strength without any improvement in columns stiffness.

On the other hand, Fig. 21 show that for RHS 80x40x3.0 section column with the same web opening ratio of 60%, an opposite behavior observed, strengthening with doubler S=2d improves only the axial compressive strength without any improvement in columns stiffness, whereas columns strengthening with doubler S=3d improves both axial compressive strength and axial stiffness.

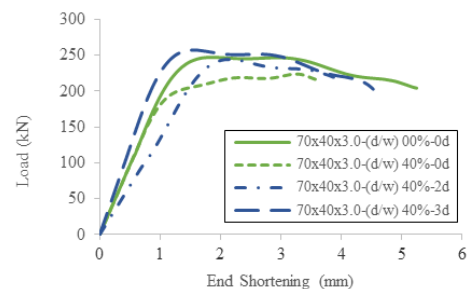


Figure 18. Load – End Shortening curve for 70x40x3.0 40%

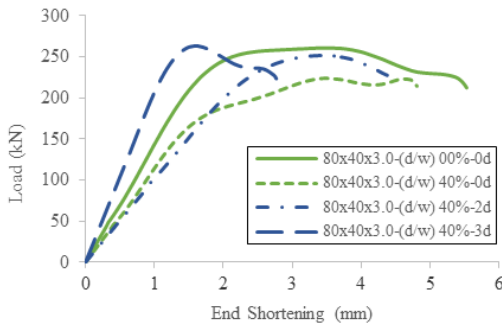


Figure 19. Load – End Shortening curve for Specimen 80x40x3.0 40%

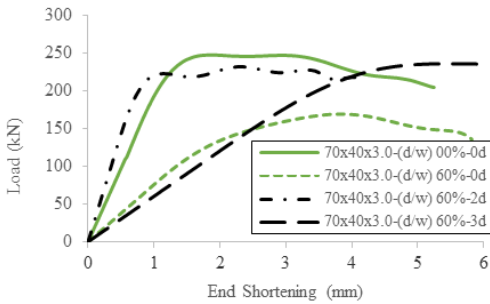


Figure 20. Load – End Shortening curve for Specimen 70x40x3.0 60%

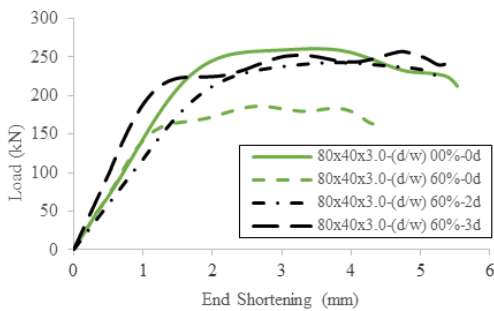


Figure 21. Load – End Shortening curve for Specimen 80x40x3.0 60%

The reason for this behavior can be justified by the effect of decreasing the axial stiffness as the cross-sectional area decreases due to the wide opening ratio being 60% rather than 40%. Also, the columns became more vulnerable to local buckling. Beside to the effect of doubler plate height relative to the specimen constant height and its effect on location of local buckling and failure mode shape and its behavior.

**4. CONCLUSION**

Fourteen cold-formed steel RHS stub columns have been experimentally tested against axial compression load

**List of symbols:**

B	Width (mm)	D	Depth (mm)
t	Thickness (mm)	d	Diameter of opening (mm)
w	Flat width (mm)	r	Outer corner radius (mm)
L	Stub column height (mm)	E	Young's modulus (GPa)

conducted in the Civil Engineering lab, at El-Azhar University. The steel column specimens that were tested have a box section with two different dimensions; seven specimens have a box section with dimensions of RHS (70×40×3) mm. The other seven specimens have a box section with dimensions of RHS (80×40×3) mm. The effect of the size of two opposing central circular web opening diameter was investigated. Specimens were strengthened with doubler plates with different heights, 2d and 3d, to investigate their effect on the axial compressive strength and stiffness of the steel columns. The specimens were divided into three groups.

**Group I:** comprise stub columns specimens without strengthening, including the reference column that has no web openings.

**Group II:** strengthened specimens by adding doubler plate with height S=2d.

**Group III:** strengthened specimens by adding doubler plate with height S=3d.

The load - end shortening curves of the stub columns and typical failure modes observed from the present test program are investigated in this research. The measured ultimate capacity of strengthened members is used to estimate the effect of the strengthening with doubler plate, with two heights 2d and 3d. Conclusions derived from this study are:

- i) The reduction in maximum axial capacity of the column based on actual test results for 40% and 60% perforation size ratio (d/w) is approximately 12% and 30% respectively. A mild drop in the load capacity of the perforated stub columns is observed as the perforation ratio, d/w, increases from 0.4 to 0.6.
- ii) Strengthening the stub columns with opening ratios 40% to 60% using doubler plates with height S=2d, increases the ultimate column capacity by about 10% to 30%, respectively.
- iii) Strengthening the stub columns with opening ratios 40% to 60% using doubler plates with height S=3d, increases the ultimate column capacity by about 17% to 40%, respectively.
- iv) Finally, the use of doubler plates in this research improved the behavior of the specimens with opening as they provide about 96% of the ultimate column capacity of the closed column.



$\sigma_0$	Yielding stress (MPa)	$\sigma_u$	Ultimate stress (MPa)
$P_{Exp.C}$	Experimental ultimate load for the closed stub column specimen (kN)	$\Delta$	End shortening (mm)
$P_{Exp.O}$	Experimental ultimate load for the perforated specimen (kN)	$P_{Exp.S}$	Experimental Ultimate load for strengthened specimen (kN)
$P_n$	Nominal load for solid specimen according to AISI-2001 [34] (kN)	R	Reduction factor ratio

## 5. References

- [1] L. Gardner, N. Saari, F. Wang, "Comparative experimental study of hot-rolled and cold-formed rectangular hollow sections", 2010, *Thin Walled Struct.*, pp. 495–507."
- [2] J. Wardenier, J.A. Packer, X.L. Zhao, G.J. Van der Vegte, "Hollow Sections in Structural Applications, Bouwen met Staal Rotterdam, The Netherlands.", 2002.
- [3] C.D. Moen, B.W. Schafer, "Direct strength method for design of cold formed steel columns with holes", 2011, *J. Struct. Eng.* (137) pp. 559–570.
- [4] J.K. Sonu, K.D. Singh, "Shear behavior of single perforated lean duplex stainless steel (LDSS) rectangular hollow beams", 2017, *Thin Walled Struct.* (119) pp. 851–867.
- [5] N.E. Shanmugam, M. Dhanalakshmi, "Design for openings in cold-formed steel channel stub columns", 2001, *Thin-Walled Struct.* (32) pp. 961–981.
- [6] N.E. Shanmugam, V. Thevendran, Y.H. Tan, "Design formula for axially compressed perforated plates", 1999, *Thin-Walled Struct.* (34) pp. 1–20.
- [7] R. Feng, B. Young, "Experimental investigation of aluminum alloy stub columns with circular openings", 2015, *J. Struct. Eng.* (141) 4015031.
- [8] R. Feng, X. Mou, A. Chen, Y. Ma, "Tests of aluminum alloy CHS columns with circular openings", 2016, *Thin Walled Struct.* (109) pp. 113–131.
- [9] Z. Yao, K.J.R. Rasmussen, "Inelastic local buckling behavior of perforated plates and sections under compression", 2012, *Thin Walled Struct.* (61) pp. 49–70.
- [10] Z. Yao, D. Ph, K.J.R. Rasmussen, M. Asce, "Perforated cold-formed steel members in compression. I: parametric studies", 2016, *J. Struct. Eng.* (143) 4016226.
- [11] T. Kumai, "Elastic stability of the square plate with a central circular hole under edge thrust", 1951, in *Proc. Japan Nat. Cong. Appl. Mech.*, pp. 81–86.
- [12] U.-N. Kim, I.-H. Choe, J.K. Paik, "Buckling and ultimate strength of perforated plate panels subject to axial compression: experimental and numerical investigations with design formulations", 2009, *Ships Of shore Struct.* (4) pp. 337–361.
- [13] W.-W. Yu, C.S. Davis, "Cold-formed steel members with perforated elements", 1973, *J. Struct. Div.* (99) pp. 2061–2077.
- [14] C.D. Moen, "Direct Strength Design of Cold-formed Steel Members with Perforations", 2008, *Civil Engineering*, Johns Hopkins University.
- [15] M. Shariati, M.M. Rokhi, "Numerical and experimental investigations on buckling of steel cylindrical shells with elliptical cutout subject to axial compression", 2008, *Thin Walled Struct.* (46) pp. 1251–1261.
- [16] C.D. Moen, B.W. Schafer, "Experiments on cold-formed steel columns with holes", 2008, *Thin-Walled Struct.* (46) 1164–1182.
- [17] K.R. Umbarkar, L.M. Patton, K.D. Singh, "Effect of single circular perforation in lean duplex stainless steel (LDSS) hollow circular stub columns under pure axial compression", 2013, *Thin Walled Struct.* (68) pp. 18–25.
- [18] N.S. Marshall, G.N. Nurick, "The effect of induced imperfections on the formation of the first lobe of symmetric progressive buckling of thin-walled square tubes", 1970, *WIT Trans. Built Environ.* 35.
- [19] Y. Pu, M.H.R. Godley, R.G. Beale, H.H. Lau, "Prediction of ultimate capacity of perforated lipped channels", 1999, *J. Struct. Eng.* (125) pp. 510–514.
- [20] M. Dhanalakshmi, N.E. Shanmugam, "Design for openings in equal-angle cold-formed steel stub columns", 2001, *Thin-Walled Struct.* (39) pp. 167–187.
- [21] North American Specification (NAS), "North American Specification for the Design of Cold-Formed Steel Structural Members", 2007, American Iron and Steel Institute, Washington, DC., USA, (AISI S100-2007).
- [22] North American Specification (NAS), "North American Specification for the Design of Cold-Formed Steel Structural Members", 2012, American Iron and Steel Institute, Washington, DC., USA, (AISI S100-2012).
- [23] Cold-formed steel structures, "Australian/New Zealand Standards", 2005, NSW, Australia, (AS/NZS 460)
- [24] Z. Yao, K.J.R. Rasmussen, "Design of Perforated thin-walled steel columns", *Research Rep.* R949.
- [25] Tekcham Gishan Singh and Konjengbam Darunkumar, "Experimental investigation on performance of the perforated cold-formed steel tubular stub columns", 2018.
- [26] Tekcham Gishan Singh and Konjengbam Darunkumar, "Capacity of cold-formed steel hollow stub columns With central circular perforations", 2018.
- [27] Tekcham Gishan Singh and Konjengbam D. Singh, "Design Of Perforated Cold-Formed Steeltubular Stub Columns – DSM Approach", 2019.
- [28] Woo Yian Peen, Choong Kok Keong, Omid Hassanshahi, "Behaviour of hollow circular section with multiple perforations under Compression, flexure and torsion", 2019.
- [29] Sadjad Amir Al-Jallad and Haitham Al-Thairy, "Effect of web opening on the axial load capacity of steel columns with cold formed thin-walled section (cfs)", 2016.
- [30] Bassem M. Dawod, "Experimental and Numerical Investigation on Strength of Eccentrically Loaded Steel Square Hollow Sections", 2021.
- [31] Kazuya Mitsui, Atsushi Sato, Massimo Latour, Vincenzo Piluso and Gianvittorio Rizzano, "Experimental Analysis and FE Modeling of Square Hollow Sections Under Combined Axial and Bending Loads", 2017.
- [32] Marsel Garifullin, Alexey Sinelnikov, Maria Bronzova St.Petersburg Polyte and Nikolai Vatin, "Buckling Behavior of Perforated Cold-formed Columns", 2019.
- [33] Gregory J. Hancock, Thomas M. Murray, Duane S. Ellifritt, "Cold-Formed Steel Structures to the AISI Specification", 2001, ISBN: 0-8247-9294-7.
- [34] North American Specification (NAS), "North American Specification for the Design of Cold-Formed Steel Structural Members", 2016, American Iron and Steel Institute, Washington, DC., USA, (AISI S100-2016).
- [35] Tekcham Singh, Konjengbam Singh, "Structural performance of YSt–310 cold-formed tubular steel stub columns", 2017.